Efficient removal of perfluorobutanesulfonic acid from water through a chitosan/polyethyleneimine xerogel

Chemical Engineering Journal 466 (2023) 143236

Contents lists available at ScienceDirect

Chemical Engineering Journal

journal homepage: www.elsevier.com/locate/cej

Efficient removal of perfluorobutanesulfonic acid from water through a chitosan/polyethyleneimine xerogel

Mohammad Reza Shirzad Kebria [a,*], Luca Bono [b], Saeed Khoshhal Salestan [c], Andrea Armirotti [d], Riccardo Carzino [a], Athanassia Athanassiou [a], Despina Fragouli [a,*]

[a] Smart Materials Group, Istituto Italiano di Tecnologia, via Morego 30, 16163, Genoa, Italy
[b] Medicinal Chemistry for Drug Discovery and Delivery, Istituto Italiano di Tecnologia, via Morego 30, 16163, Genoa, Italy
[c] Department of Chemistry and Chemical Engineering, Chalmers University of Technology, Gothenburg SE-412 96, Sweden
[d] Analytical Chemistry Facility, Istituto Italiano di Tecnologia, via Morego 30, 16163, Genoa, Italy

ARTICLE INFO

Keywords:
Perfluoroalkyl substances (PFASs)
Water remediation
Adsorption
Molecular dynamics

ABSTRACT

Due to the recently ratified legislations, the use of long-chain poly- and perfluoroalkyl substances (PFASs) must be reduced and in the absence of a safe alternative, short-chain PFASs are currently used in their place. The continuously growing utilization of the short-chain PFASs, results in their abrupt introduction in the environment, and highlights the importance of adopting efficient remediation strategies. This study addresses an appropriate solution to remove perfluorobutanesulfonic acid (PFBS) from aqueous media through a static adsorption process. Specifically, a chitosan/polyethyleneimine based composite xerogel was prepared and its ability to remove PFBS from water was studied in detail. Behavioral patterns of the PFBS adsorption process were perused over a broad range of concentrations from ppb to ppm, and the adsorption studies reveal that the maximum PFBS adsorption capacity reaches up to 305 mg/g within 24 h from the beginning of the process. In addition to the electrostatic interaction between the amine groups of the xerogels and the negatively charged PFBS molecules, the formation of hydrogen bonds were also revealed by the chemical characterization and confirmed by molecular dynamics simulation studies.

1. Introduction

Poly- and perfluorinated alkyl substances (PFASs) are chemically inert and thermally stable organofluorine synthetic compounds owning multifold fluorine atoms, with short C-F bond length and high bond energy, low molecular polarity and amphiphilicity [1–3]. Due to their interesting properties, for several decades they have been extensively used in diverse consumer and industrial product applications such as cookware, disposable food packaging, furniture and carpet coatings, as surfactants in paintings, additives in production of firefighting foams etc. [4,5]. Nonetheless, their thermal and chemical stability makes also PFASs extremely stable when exposed to the environment, transforming them into persistent environmental pollutants found in groundwater and surface waters, treated drinking water, rainwater, snow, but also in municipal sewage, in biosolids, landfill leachates etc. [6]. Their high persistence and water mobility, in combination with the inappropriate remediation approaches result in their high interaction with living organisms and eventually with humans. In fact, studies have shown that PFASs bioaccumulate, causing serious acute and chronic health effects, such as liver and kidney malfunction, endocrine dysfunctions, pediatric allergies, cardiovascular diseases, immune toxicity, while tests on animal models have connected them to the high risk for cancer [7,8].

To deal with this issue, diverse legislation actions have banned the use of long-chain PFASs, and instead fluoroalkyl compounds of shorter chains have been proposed. Indeed, due to the lack of harmless alternatives, long-chain PFASs have been substituted by congener molecules of shorter-chains such as perfluorobutanoic acid (PFBA) and perfluorobutanesulfonic acid (PFBS) among others. Specifically the short-chain PFBS, as a four-carbon containing cognate of perfluorooctanesulfonic acid (PFOS), has been extensively used as its substitute due to its shorter biological half-life in humans (~1 month vs 5 years for PFOS) [9,10]. Nonetheless, from a technical point of view, due to their shorter chains, higher amounts are needed for comparable, to their long-chain PFASs counterparts, performances [11]. Therefore, the higher amounts of short-chain PFASs used in combination with their high mobility in water, turn them into potentially hazardous

* Corresponding authors.
E-mail addresses: mohammad.shirzad@iit.it (M.R. Shirzad Kebria), despina.fragouli@iit.it (D. Fragouli).

https://doi.org/10.1016/j.cej.2023.143236
Received 3 February 2023; Received in revised form 28 March 2023; Accepted 26 April 2023
Available online 2 May 2023

environmental pollutants that might behave similarly in terms of persistence and bio-accumulation as the longer-chain PFASs [12].

Among diverse remediation processes for PFASs removal, such as electrocoagulation, biological degradation, oxidation and membrane separation [11,13–15], adsorption is possibly the most promising due to its high elimination rate, simplicity, and reasonable operational costs. Nevertheless, although there are many adsorption studies for various types of long-chain PFASs, e.g. perfluoroalkyl acids (PFAAs), using conventional sorbents such as carbon-based materials (granular activated carbon, carbon nanotubes) and anion-exchange resins [16], the removal of short-chain counterparts still needs extensive investigation [17–19]. Therefore in the last years various types of materials in the form of particles, such as metal organic or cationic covalent-organic frameworks, have been developed [20–23], or other remediation methods like sono-chemical decomposition and ultraviolet-induced photo degradation [24,25] have been applied for the effective remediation of short-chain PFAS molecules. Nonetheless, their large scale application may be limited by the additional post-processing steps needed for the removal of the powder based sorbents from the treated solutions though centrifugation or filtration in the former, and by the long interaction time, high energy demand, and complexity of operation in the latter case.

Recently, polymer based adsorbents have attracted significant attention due to their biocompatibility, versatility, and abundant surface functional groups. Specifically for the PFBS removal, adsorbents able to interact with both the hydrophilic anionic sulfonate head group and the hydrophobic perfluorinated end group may offer a more efficient remediation performance. In fact, electrostatic interactions between a positively charged sorbent and the anionic head group as well as formation of hydrogen bonds can be expected during the adsorption process. Following this approach, Huang et al. developed functional hydrogels through both fluoridation and amination of polyethylene glycol diacrylate, for the effective sorption of PFBS from aqueous solutions reaching an adsorption capacity of 50 mg/g and removal efficiency of 95% after 6 h of interaction with a PFBS solution (initial concentration: 111.5 mg/l) [1]. In another study, Ateia et al. synthesized a poly (N-[3-(dimethylamino)propyl]acrylamide-methyl chloride quaternary) hydrogel as an efficient adsorbent for the elimination of PFBS from various water matrices reaching a PFBS removal efficiency higher than 90% after 24 h of interaction (initial PFBS concentration: 1 mg/l) [26]. Overall, functional hydrogels have been proved to be efficient sorbents for such type of molecules, due to their high water retention which allows pollutants in water to diffuse easily into their bulk structure, and due to their low cost and their facile functionalization for optimum results. Sorbents containing amine groups present an effective interaction with the anionic compounds [27–29]. In particular, polyethyleneimine (PEI) demonstrates an excellent performance for the adsorption of heavy metals [30,31], anionic organic pollutants [32], and volatile organic compounds [33] due to the abundance in primary and secondary amine groups that can be protonated in a wide pH range. For example, PEI-functionalized cellulose microcrystals (PEI-f-CMC) were able to remove diverse types of PFAS compounds with significantly higher efficiency compared to the non-functionalized CMC demonstrating the importance of the role of PEI in the whole process [34]. On the other hand, chitosan (CS) as a natural biodegradable, non-toxic and hydrophilic amine (–NH_2) and hydroxyl (–OH) containing bio adsorbent [35–37] is expected to further enhance the adsorption capacity of PEI [38]. On the top, as proved by Zhang et al. CS beads of 2–3 mm could effectively remove PFBS molecules with an adsorption capacity of 1 mmol/g in acidic media (pH = 3) after 11 h, due to the electrostatic interaction with the functional groups of the CS structure [39]. Therefore, combining PEI and CS to form a three-dimensional (3D) framework with high porosity can be a key to success in the adsorption of short-chain PFASs.

In this work, a CS/PEI composite xerogel was prepared through a cryogelation process to adsorb PFBS. The prepared xerogel had the ability to swell and absorb water up to 30 times relative to its weight. The structural and physicochemical properties of the prepared adsorbent were assessed using scanning electron microscopy (SEM), X-ray photoelectron spectroscopy (XPS) as well as Fourier transform infrared spectroscopy (FTIR). The Brunauer-Emmett-Teller (BET) method was applied to determine the surface area of the synthesized xerogel. The adsorption mechanism and governing kinetics theory were investigated while the interaction between the PFBS molecules with composite xerogels was simulated via molecular docking. The performed study demonstrates that the as prepared CS/PEI xerogel can efficiently remove PFBS from water with a maximum adsorption capacity of 305 mg/g, through electrostatic and hydrogen bond interactions. The outcomes of this work are expected to be a motivation for the development of analogous 3D polymer based adsorbent blocks for the remediation of various members of the short chain PFASs family in water.

2. Materials and method

2.1. Chemicals and reagents

PEI (average Mw ~ 750,000, 50 wt% in H_2O), CS powder (medium molecular weight, 75–85% deacetylated), glacial acetic acid (Ph. Eur., ≥99.8%), 1,4-Butanediol diglycidyl ether (BDDE, purity ≥ 95%) and PFBS (97%) were purchased from Sigma-Aldrich and used without further purification.

2.2. Preparation of the CS/PEI composite xerogel

To prepare the CS/PEI xerogel, 1 ml of PEI was added to 9 ml deionized (DI) water and the mixture was stirred for 15 min. Simultaneously, 0.5% w/v CS solution was prepared by dissolving CS in a solution containing 0.2 ml acetic acid and 9.8 ml DI water. Then, the CS solution was added to the PEI solution in different volumetric ratios (CS: PEI 1:9, 3:7, 5:5 and 0:10 for the pure PEI xerogel) and the resulting mixture was stirred until a homogenous solution was reached. To initiate the crosslinking procedure, various amounts of BDDE (200, 400, and 500 µl) were added to the CS/PEI prepared solutions (10 ml). Then, the solutions were vortexed for 15 sec and instantly pipetted into soft straws before storing for 18 h at −18℃ to attain cryo-crosslinking. After 18 h, the obtained cylindrical gels were rinsed three times with DI water, and then they were dried in an air oven at 55℃ for 18 h. Subsequently, the samples were dipped in DI water for 5 min in order to remove the non-reacting components, and then dried. To choose the optimum composition, the prepared xerogels were submerged in DI water for different durations (1, 3, 5 min) in order to define their water uptake capacity and stability (Supporting Information, Fig. S1). The higher the water uptake and the water stability of the composite, the higher and more effective is the contact of its active sites with the pollutants, leading to a better overall performance. Through this preliminary study, the 0:10 CS/PEI and 1:9 CS/PEI with 200 µl of BDDE were chosen for further experiments.

2.3. Characterization

SEM (JEOL JSM-6490LA, with accelerating voltage of 5 kV) equipped with an energy-dispersive X-ray spectroscopy system (EDS) was applied to assess the structural properties of the prepared xerogels, and their modification after the PFBS adsorption process. All specimens were covered with an Au coating (thickness of 10 nm) using the high-resolution sputter coater Cressington 208HR (Cressington Scientific Instrument Ltd., UK). To investigate the mean pore size distribution of the prepared CS/PEI xerogel in detail, ImageJ software was employed to analyze the SEM images. The reported mean values are the average values of 650 points for internal pores and the area of 385000 μm^2 for macropores.

A single-reflection attenuated total reflection (ATR) accessory

(MIRacle ATR, PIKE Technologies) coupled to an FTIR spectrometer (Vertex 70v FT-IR, Bruker) (ATR-FTIR) and XPS were employed for the investigation of the chemical properties of the xerogels, and for the characterization of the chemical interactions between the xerogel's components and of the adsorbed PFBS molecules. The ATR-FTIR spectra were averaged from 128 repetitive scans recorded in the range from 4000 to 600 cm^{-1} with a resolution of 4 cm^{-1}. XPS analysis was performed using an electron spectrometer (Lab2, Specs, Berlin, Germany) equipped with a monochromatic X-ray source (set at 1486 eV) and with a hemispherical energy analyzer (Phoibos, HSA3500, Specs). The operational voltage of the Al Kα X-ray source and the functional current were adjusted at 13 kV and 8 mA, respectively. The pressure in the analysis chamber was $\sim 1 \times 10^{-9}$ mbar. The large area lens mode was used for both wide and narrow scans. For the wide scan, the energy pass was 90 eV and the energy step was 1 eV. For the narrow high-resolution scan, the energy pass was 30 eV and the energy step was 0.1 eV. A flood gun was used to neutralize the surface charge, having an energy of 7 eV and a filament current of 2.2 A. Thermogravimetric analysis (TGA) and derivative thermogravimetry (DTG) were carried out by means of TGA Q500 system (TA Instruments, USA) at a ramp rate of 10℃/min from 30 to 800℃ in nitrogen atmosphere. The nitrogen adsorption–desorption analysis was performed using a surface area analyzer (Autosorb iQ Quantachrome). The specific surface area was obtained by the BET theory. In addition, the Barrett-Joyner-Halenda (BJH) model was applied to determine the pore size distribution in the nanometric range. For this reason, BJH model was used on the desorption band of the isotherm for the relative pressure of $P/P^o > 0.35$.

The xerogel's interactions with water were specified using gravimetric and volumetric analyses. To determine the swelling degree of the xerogels, a dried gel specimen with certain volume (110 mm^3) was subjected to DI water bath. The swelling degree and water uptake of the xerogels were determined by measuring the cumulative mass and volume increase at specific time intervals. Excess water was leniently removed from the whole area of the samples by means of a moist and soft paper tissue before measuring the mass and volume of the swollen xerogel. Then, the gravimetric and volumetric swelling degree were defined as a ratio of the mass and volume of the swollen xerogel to the dry sample, respectively.

2.4. Adsorption experiments

For the adsorption experiments, PFBS solutions with various concentrations varying from ppb to ppm were prepared. For each concentration, three xerogel specimens with similar weight and dimension (weight ~22.5 mg and volume ~110 mm^3 for the dry samples) were selected. In brief, adsorption kinetics evaluation was carried out by dipping the xerogels to 13 ml solutions containing PFBS at various concentrations (from 10 ppb to 600 ppm) with pH of around 6.5. For each case, aliquots from the solution were collected at specific time intervals (from 0.5 to 100 h) and the PFBS concentration variation from the initial one was defined. The adsorption process took place at static conditions and at room temperature. For each case, adsorption tests were carried out in triplicate and the mean value for each parameter is presented.

To calculate the adsorption capacity of each sample, the following equation was employed:

$$q_{(t)} = \frac{(C_0 - C_{(t)})}{m} \times V \quad (1)$$

Where q_t ($mg_{PFBS}/g_{xerogel}$) is the adsorption capacity at the time t, C_0 and $C_{(t)}$ (mg/L) represent the initial concentration and the concentration at the time t of the PFBS, V (L) is the volume of PFBS solution, and m (g) is the mass of the dry xerogel.

The adsorption kinetics were investigated by applying the pseudo-first-order (Equation (2)) and the pseudo-second-order (Equation (3)) kinetics models on the experimental data obtained at different PFBS C_0.

$$\mathrm{Ln}\,(q_e - q_t) = \mathrm{Ln}q_e - K_1 t \quad (2)$$

$$\frac{t}{q_t} = \frac{1}{K_2 q_e^2} + \frac{t}{q_e} \quad (3)$$

where q_e and q_t (mg/g) are the adsorption capacity at the equilibrium and at time t (min), respectively, while K_1 (L/min) is the pseudo-first-order and K_2 (g/mg•min) the pseudo-second-order rate constant [40,41]. The adsorption data were fitted with various isotherm models, in their nonlinear forms, in order to explore possible interaction mechanisms between the PFBS and the adsorbent.

2.5. Analytical measurements

Quantification of PFBS was carried out on a Waters Acquity UPLC system coupled with a Xevo TQ-MS triple quadrupole mass spectrometer equipped with an Electrospray Ionization ion source. After dilution with water to a suitable final concentration, samples were run on a reversed-phase BEH C18 column (2.1x50 mm, 1.7 μm) with a VanGuard BEH C18 pre-column (2.1x5 mm, 1.7 μm). The temperature was kept at 45 °C, and the flow rate at 0.500 ml/min. Elunets were 10mM NH_4OAc in H_2O at pH 5 adjusted with CH_3COOH (A) and 10 mM NH_4OAc in CH_3CN-H_2O (95:5) at pH 5 (B) as mobile phase. A linear gradient was applied where B increased from 5 to 95% in 3 min. Total run time was 4.50 min. The mass spectrometer operated in the negative ESI mode and PFBS was quantified by multiple reaction monitoring (MRM). The tracked transitions from precursor to product ion were the following: 299->80 *m/z* (collision energy 50 eV) and 299->99 *m/z* (collision energy 25 eV). The capillary and the cone voltages were set at 3 kV and 30 V for both transitions. The source temperature was set to 120 °C. Desolvation and cone gas flows (N_2) were set to 800 and 50 l/h, respectively. Desolvation temperature was set at 450 °C. Sample concentration was evaluated on the basis of the analyte peak area compared with standard curve peak areas. Data were quantitatively analyzed used Targetlynx software. The concentration of PFBS in the samples was calculated using an external calibration curve.

2.6. Molecular simulation

To assess the adsorption mechanism, a polymeric composite comprising PEI and CS (as pristine adsorbent) was selected to construct a simulation box. Molecular dynamics simulation was conducted using Materials Studio 6.0 software and employing COMPASS force field to reach an equilibrium structure [42]. The Method of 'Charge Qeq' was nominated to set electrostatic charge of atoms while Ewald summation method with accuracy of 10^{-5} kcal/mol was applied for the calculation of the electrostatic interactions. In addition, van der Waals interaction was taken into consideration based on the atom-based technique, while cutoff distance was set on 18 Å. Afterwards, the molecular docking was implemented by the use of AutoDock Vina software [43] to compute the intermolecular interactions between PFBS and the active sites of the adsorbent.

To begin the molecular simulation, one chain of CS and one of PEI including 65 and 250 monomers, respectively, were built using "build module". The molecular weight of CS and PEI chain were determined to be 10447.2 and 10769.3 g/mol, respectively. Then, a simulation cell was created using the afore-produced chains and employing an "amorphous cell module". The simulation cell was called 'composite'. The equilibrium structure of the composite was achieved by following a pattern of consecutive dynamic runs at NPT (number of the particles, temperature, and pressure are constant) ensemble which consist of: a) 100 ps NPT run at 1 bar and 298 K; b) 100 ps NPT run at 1 bar and 600 K; c) 100 ps NPT run at 10000 bar and 600 K; d) 100 ps NPT run at 10000 bar and 298 K; e) 100 ps NPT run at 1 bar and 298 K. The mentioned order was replicated ten times to ensure that the equilibrium structure was achieved. Once the equilibrium is achieved, the ultimate snapshot was captured as

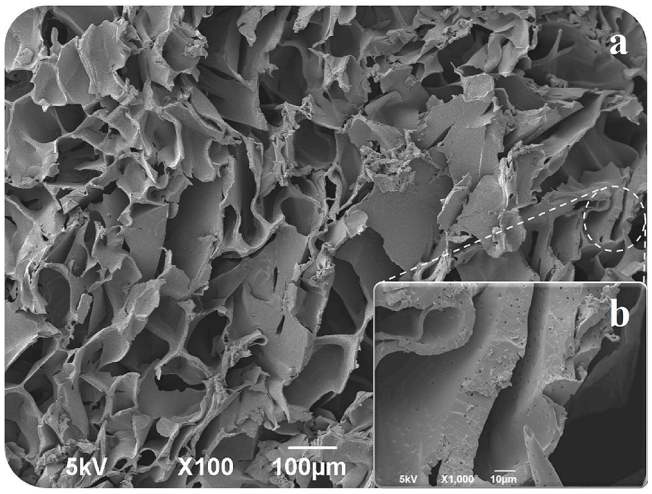

Fig. 1. SEM image of the prepared CS/PEI composite xerogel (a) and higher magnification of the selected cell wall (b).

the 3D model for the molecular docking calculation. The chains of CS and PEI, the atomic structure of PFBS, and the equilibrium simulation cell were visualized in Fig. S2 of the Supporting Information file. The ultimate snapshot and the optimized molecular structure of PFBS, which was attained by using "geometry optimization module", were saved as mol2 format, and then they were converted to the PDBQT format applying AutoDock software. The electric charge of atoms was maintained in mol2 files and non-polar hydrogens were removed from the structure. A suitable 30 × 30 × 30 site was opted with Grid box and the PDBQT files were called by AutoDock vina to perform molecular docking.

3. Results and discussion

The morphology of the cylindrical shaped xerogel, explored with SEM (Fig. 1) reveals that it has an open macroporous structure with interconnected pores with mean pore size of 82.65 ± 33.2 μm, surrounded by thick pore walls (indicative pores thickness 13–16 μm). As shown in the inset of Fig. 1, the pore walls are not compact, but they present smaller pores of around 209 ± 101 nm proving that the developed xerogel is a porous material with dual porosity.

The specific surface area in the nanometric range of the prepared xerogels was calculated through adsorption–desorption nitrogen isotherms, using the BET theory. As shown in the Supporting Information Fig. S3, and according to the IUPAC classification, the shape of the N_2 adsorption–desorption is a combination of type II and type IV isotherms, with the type II isotherm to designate the unlimited monolayer-multilayer adsorption, and the type IV isotherm to describe its hysteresis loop [44]. Type IV isotherm suggests that the nanometric pores belong to the mesopore (2 – 50 nm) and macropore (>50 nm) size range [45], while the BET specific surface area was found to be 2.148 m^2/g. These characteristics are in agreement with other similar 3D porous materials containing CS, PEI, or both simultaneously [46–48]. Small differences can be attributed to the materials composition, drying procedure, or other operational parameters.

The xerogel's interaction with the water is studied through the definition of the gravimetric and volumetric swelling degrees. With the volumetric swelling degree the size expansion of the gel, only due to the uptake of water by the polymeric network is defined, while the gravimetric swelling degree includes both, the mass of water in the polymeric network and in the region of the pores [49]. The gravimetric swelling degree of the xerogel was 30 g/g, significantly higher compared to the volumetric swelling degree (2.5 cm^3/cm^3) possibly due to the physical spatial constraints imposed by the crosslinking of the polymer macromolecular chains that limit their mobility. The gravimetric swelling degree analysis was repeated after drying the sample at room temperature for 72 h, and as shown in Fig. S1 where the wetting properties of xerogels of different combinations of CS, PEI and BDDE were explored, the xerogel of the defined composition (1:9 CS/PEI- 200 μl of BDDE) showed a similar performance indicating its stability in aqueous media.

To evaluate the thermal properties of the CS/PEI xerogel, TGA analysis was performed in comparison with the pure CS powder, and the PEI xerogel. As presented in Fig. 2, the first degradation step for all samples tested is at low temperatures, below 100 °C, which can be generally attributed to the desorption of adsorbed humidity. For the PEI and CS/PEI xerogels a second degradation step is observed at temperatures below 150 °C attributed to the PEI molecules of lower molecular weight than the average bulk PEI molecular weight, easily lost through volatilization [50]. From 150 °C to 300 °C, the PEI xerogels maintain an almost stable mass, while the pure CS has almost concluded its second degradation step, started at c.a. 230 °C, due to the depolymerization of the CS chains through deacetylation and cleavage of the glycosidic linkages via dehydration and deamination [51]. On the other hand, the CS/PEI xerogel follows the same degradation profile as the one of PEI, indicating the presence of strong interactions between the two polymers. Eventually, both xerogels break down at temperatures higher than 300 °C with a sharp weight loss step. At 375 °C, the samples are thoroughly decomposed and eliminated as volatiles, due to the oxidative decomposition of the organic moiety. Pure CS, though, experiences its third degradation step and decomposes completely after 600 °C due to

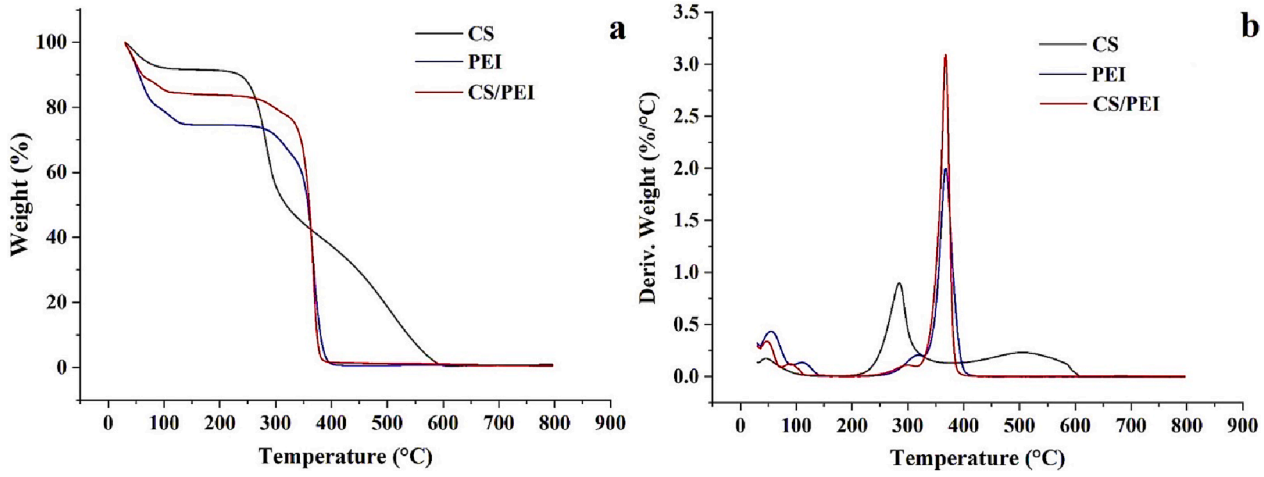

Fig. 2. TGA (a) and DTG (b) curves of pure CS, PEI xerogel, and CS/PEI xerogel.

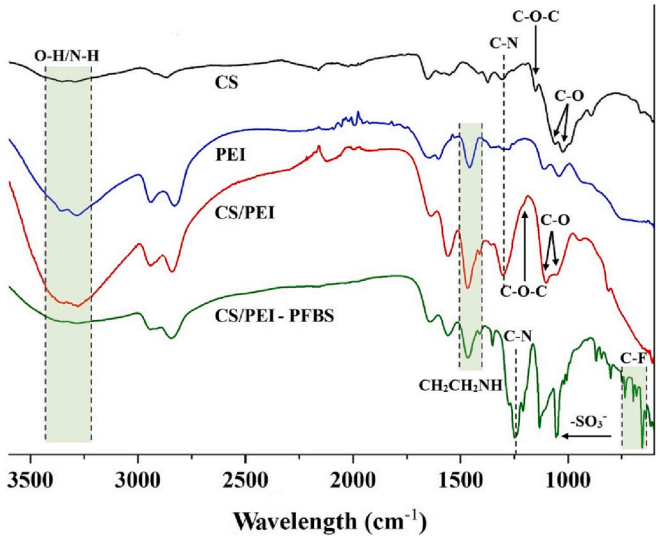

Fig. 3. FTIR spectra of pure CS, PEI xerogel, and CS/PEI xerogel before adsorption, and CS/PEI xerogel after PFBS adsorption.

the thermal destruction of the pyranose rings of the polymer [52].

The chemical interactions between the xerogel's components were defined through ATR-FTIR analysis. As shown in Fig. 3, the spectrum of the CS/PEI composite contains peaks of both polymers but also some new peaks. The broad absorption peak between 3600 cm^{-1} and 3000 cm^{-1} attributed to the N-H and O-H stretching modes is much more pronounced in the case of the CS/PEI and PEI xerogel compared to the pure CS. Based on the fact that in the TGA analysis the composite xerogel showed lower weight loss attributed to the adsorbed humidity than the PEI (Fig. 2(a)), the more pronounced FTIR peak in the case of the CS/PEI xerogel can be attributed to the higher amount of amine groups. The presence of CS in the composite xerogel can be verified by the large band located in the area of 1100 cm^{-1}, indicative of the stretching vibrations of the C-O-C bonds of the polysaccharides [52]. However, compared to the pure CS, it is evident that there is a shift towards higher frequencies, as the characteristic absorption band assigned to the asymmetric stretching of the C-O-C bridge shifts from 1151 cm^{-1} (for the pure CS) to 1203 cm^{-1} (for the CS/PEI), while the bands of CS attributed to the C-O stretching (1060 cm^{-1} and 1025 cm^{-1}) are shifted to 1100 cm^{-1} and 1050 cm^{-1} respectively in the composite xerogel indicating the modification of the environment due to the presence of the PEI [53].

On the other hand, the presence of the PEI in the composite is supported by the peaks at 1468, 1412, and 814 cm^{-1} ascribed to the vibration modes of the $–CH_2CH_2NH$ [54]. Moreover, the peaks at 1638 cm^{-1} and 1559 cm^{-1}, correspond to amide I in CS, and to the N-H bending from the amine/amide II vibration, respectively [52,55–58]. Eventually, the peak observed at 1303 cm^{-1} which is attributed to the C-N stretching vibration, is also present at the spectra of the pure CS and PEI xerogel. Nonetheless, in the case of the CS/PEI the peak is promoted indicating a good interaction between the two polymers [59,60].

To further explore the chemical interactions between the components, XPS analysis is performed. As shown in Fig. S4 of the Supporting Information, the wide scan spectra of the samples indicates that the N element contribution is enhanced in the case of the CS/PEI xerogel compared to the pure CS and PEI xerogel. In particular, the N element contribution increased from 4.3% and 9.8% for CS and PEI xerogel respectively, to 13.0% for the CS/PEI composite xerogel. Deconvolutions of the C1s high-resolution spectrum (Fig. 4(a-c)) of the pure CS, PEI xerogel and CS/PEI xerogel before adsorption reveal the different composition of the three samples. In particular, in the case of CS, three discrete peaks with binding energy (BE) at 285, 286.6, and 288.3 eV appear, which can be assigned to C-C/C-H, C-O, and O-C-O, respectively. In the C1s spectrum of the PEI xerogel, together with the C-C/C-H, two new peaks are observed at 286.1, 288.2 eV attributed to the C-N/C-O (BEs of C-N and C-O have similar values) and N-C-O. Upon formation of CS/PEI xerogel, together with the C-C/C-H, the two peaks with BE at 285.8, and 288.2 eV can be ascribed to the C-N/C-O and to the N-C-O/O-C-O of PEI/CS polymers, respectively. The nitrogen core line analyzed for CS (panel N1s, Fig. 4(e-g) divulged the BE of the primary amines (NH_2) at 399.7 eV. The N BE in the case of the PEI and CS/PEI xerogels observed at 399.2 eV, can be attributed to the secondary amines binding (N-H) confirming the conversion of primary amines of pristine CS and PEI to secondary after crosslinking. Moreover, a similar peak (NH_3^+) at ~ 401.2 eV was observed for all the samples that could be ascribed to the protonation of the abundant aliphatic amines in CS and PEI [61].

The ability of the CS/PEI xerogel to adsorb PFBS was studied by dipping it in solutions containing defined amount of PFBS that range from few ppb to hundreds of ppm. As shown in the SEM analysis of Fig. S5(c), no significant structural transformation took place after submerging the samples into a PFBS solution of 100 ppm for 24 h which confirms the stability of the produced xerogels. On the top, the presence of PFBS molecules onto the composite xerogels was corroborated by EDS analysis (Fig. S5(d)). In particular, it is detected the F element, characteristic component of the specific pollutant, homogeneously dispersed in the whole structure of the composite xerogel (Fig. S6).

The wide scan of the XPS analysis of the CS/PEI xerogel after the pollutant adsorption indicates the presence of the F and S elements which are representative of the PFBS molecule (Fig. S7). In addition, the deconvolution of the high resolution C1s peak (Fig. 4(d)) reveals the presence of the CF_2 bonds at 291.6 eV. Furthermore, as displayed in Fig. 4(h), the contribution of the NH_3^+ peak to the high-resolution N1s spectrum of the PFBS-adsorbed xerogel is higher, compared to the CS/PEI xerogel (20.7% vs 4.5%). This phenomenon implies that due to the high electronegativity of the PFBS molecules, when in contact with the xerogel, the amine groups donate and share the lone electron pair with the empty orbit of the cationic compound, featuring thus weak-base characteristics, forming protonated amine groups and favoring the electrostatic interaction with the PFBS molecules [62,63].

The FTIR analysis of the PFBS-loaded CS/PEI xerogel demonstrates the presence of various characteristic peaks of the specific molecule (Fig. 3). In particular the peak at 1274 cm^{-1}, 1210 cm^{-1} and the sharp peak at 1133 cm^{-1} are attributed to the $\nu_s(CF_2)$, while the rocking and wagging vibrations of C − F were displayed over a range from 655 to 746 cm^{-1} [1,29,64]. The peak at 1056 cm^{-1} corresponds to the $\nu_{as}(SO_3^-)$ of the PFBS, while the presence of major adsorption peaks representative of the sulfonate group, including the S = O stretching, are observed in the range of 1250–1150 cm^{-1} and 1075–1000 cm^{-1} which overlap with the defined CF assignments [1,65]. Compared to the spectrum of the CS/PEI xerogel, it is evident that the contribution of the peak attributed to the –OH and N-H groups (broad peak at c.a. 3300) is significantly reduced in the case of the PFBS-CS/PEI indicating the participation of such components to the adsorption process. Furthermore, hydrogen bindings between the PFBS molecules and composite xerogels caused a distinguished shift in the position of C-N stretching from 1303 to 1248 cm^{-1} confirming the contribution of the amine group in the adsorption process.

Overall, for the so far conducted analysis it can be concluded that the positively charged amine groups present in both PEI and CS backbone are responsible for the uptake of the short-chain negatively charged PFBS molecules likely by electrostatic interactions. On the other hand, the presence of O-H and N-H bonds in the sorbent led to formation of H–bonds among the adsorbent and the PFBS molecules.

After proving the effective adsorption of the PFBS on the CS/PEI xerogel, the time needed to reach the equilibrium is explored through the PFBS adsorption kinetics study. As shown in Fig. 5(a) the adsorption capacity evolution over time for two different concentrations of the PFBS, 500 ppb and 400 ppm is studied. At higher concentration the adsorption capacity is higher, while the PFBS adsorption seems to be

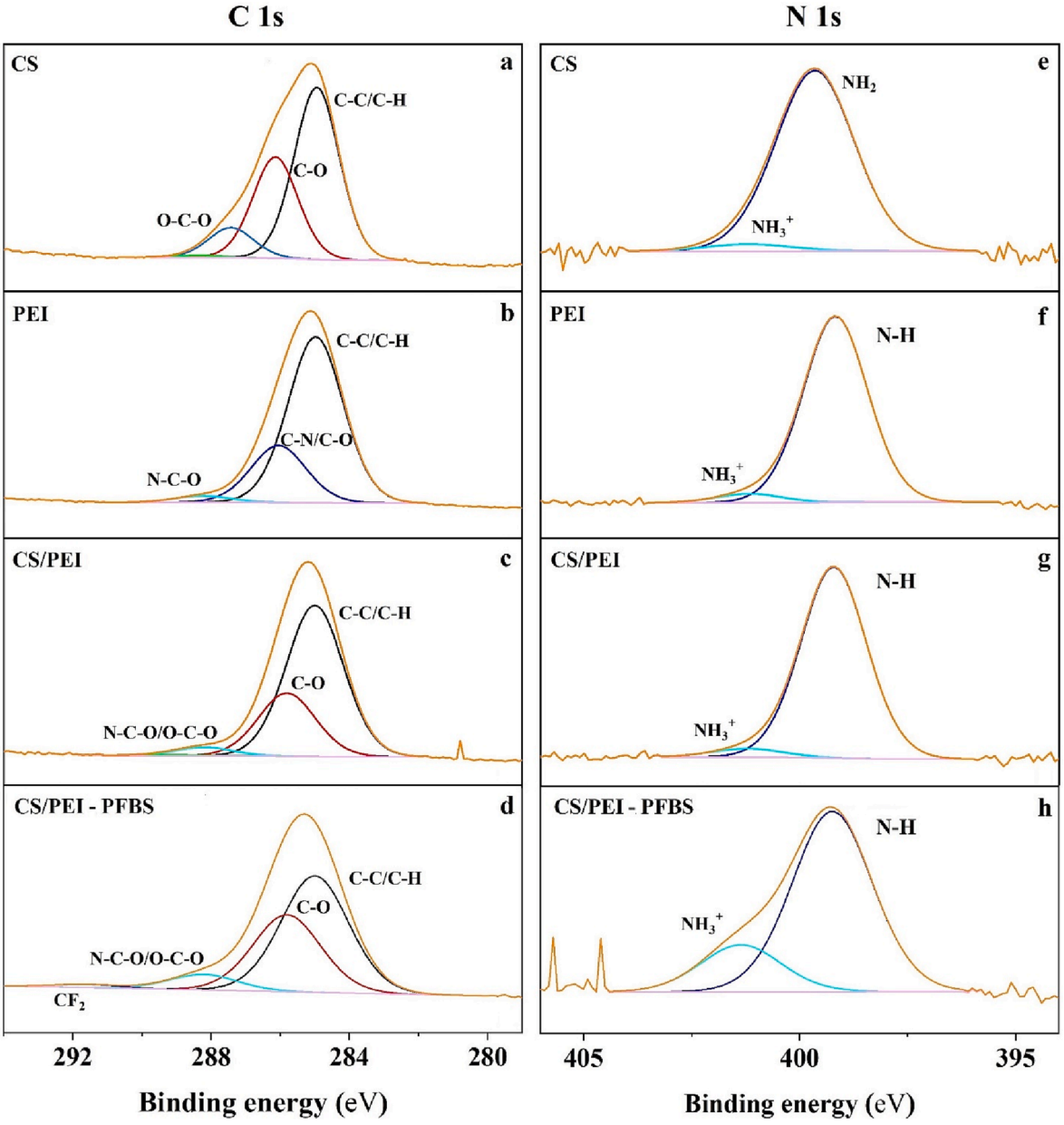

Fig. 4. Deconvolutions of XPS peaks of the C 1 s (a-d) and N 1 s (e-h) regions for pure CS, PEI xerogel, CS/PEI xerogel, and CS/PEI xerogel after PFBS adsorption, respectively.

more effective at the first hours due to the higher possibility of interaction between the adsorbent and the PFBS molecules. On the other hand, the equilibrium is reached in a slightly longer time for higher concentrations.

The empirical data were fitted by the pseudo-first-order and pseudo-second-order kinetic models in order to extract the adsorption kinetics rate, and to explore if the adsorption process is diffusion-controlled, which is well explained by a pseudo-first order rate law, or controlled by the adsorption reaction between the PFBS and the xerogel, as the pseudo-second-order kinetic model designates [66]. As can be observed in Fig. 5(a), Fig. S8, and Table S1, all data were better-fitted using the pseudo-second-order model, indicating the presence of an adsorption reaction. On the top, the reaction rates are in the range of 10^{-1}-10^{-2} for PFBS concentrations up to 5 ppm while, above 10 ppm they become slower (in the range of 10^{-3}) proving the slower adsorption performance for higher PFBS concentrations. The longer equilibrium time needed for the sorption of PFBS at higher concentration is possibly related to the complicated interactions with the xerogel, due to the rearrangement of the adsorbed molecules and the possible formation of multilayers which may block some active areas of the adsorbent, slowing down the adsorption rate [39].

The evolution of the adsorption capacity in the equilibrium, at different PFBS C_0 (Fig. 5(b)) evidences that the adsorption capacity is higher for higher C_0 reaching up to 305 ± 45 mg/g. This performance is comparable to sorbents in the powder form, despite having a significantly lower surface area (Table S2). Interestingly, in agreement with previous observations [16], two different behaviors were observed for PFBS C_0 lower than 50 ppm and for C_0 higher than 50 ppm, indicating that different adsorption mechanisms occur. To elucidate such phenomenon, as also the interactions between the PFBS and the adsorption sites of the CS/PEI xerogel, diverse adsorption isotherms have been applied for the fitting of the experimental data, such as Langmuir, Freundlich, Sips, Temkin, and Redlich-Peterson. Using a single isotherm for the data fitting in the whole concentration range was not possible,

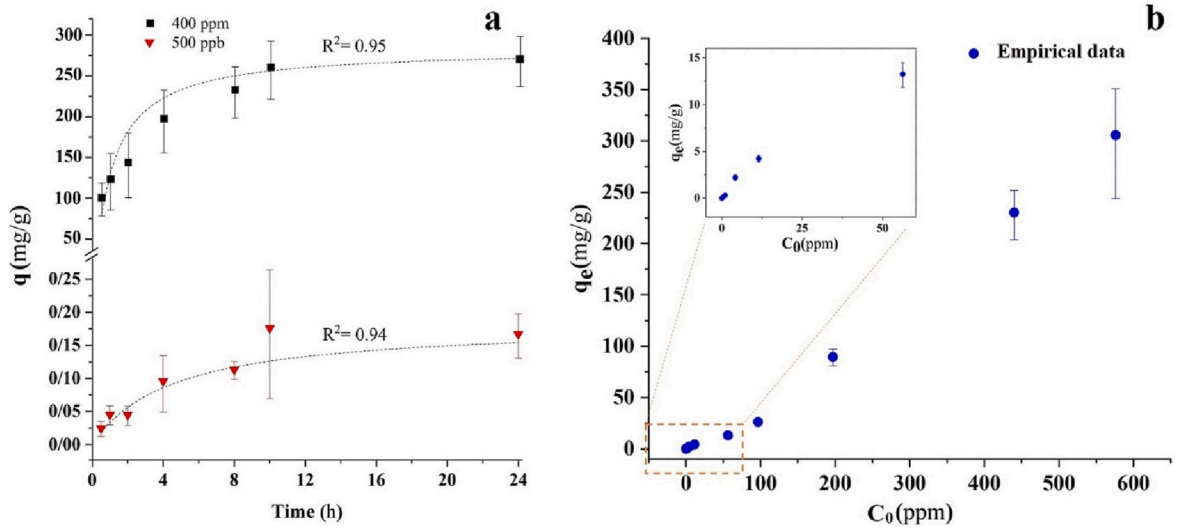

Fig. 5. Evolution of the adsorption capacity over time for PFBS concentrations of 500 ppb and 400 ppm, together with the fitting through the pseudo-second-order kinetics model (a), and PFBS adsorption capacity vs. initial PFBS concentration (b).

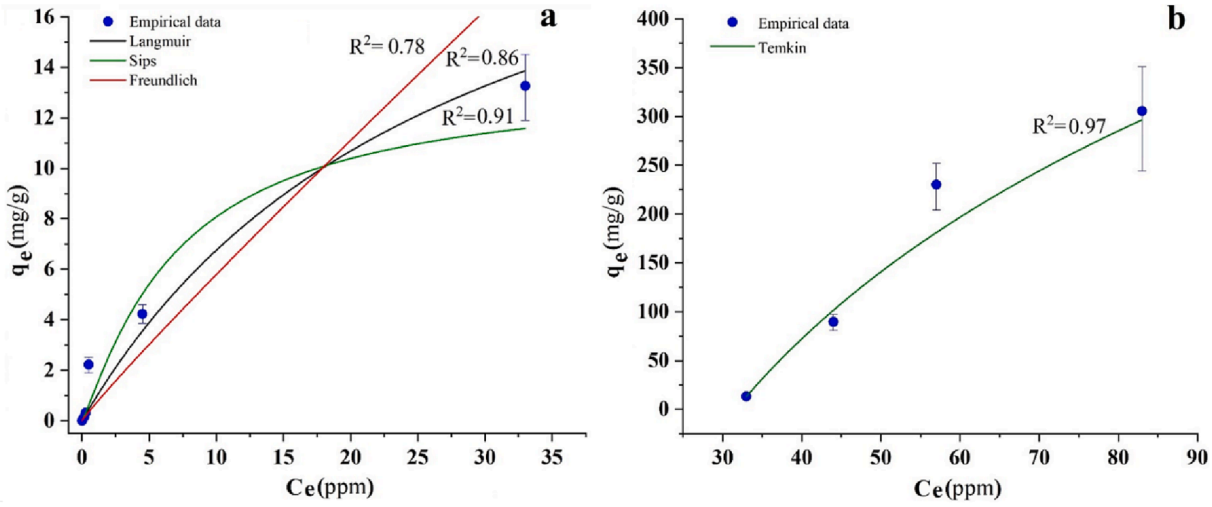

Fig. 6. Adsorption isotherms over low to moderate (a), and moderate to high PFBS concentrations (b). For $C_0 > 50$ ppm, both Langmuir and Freundlich models could not converge the empirical data.

confirming the different adsorption processes observed at the low ($C_0 <$ 50 ppm) and high concentration range ($C_0 >$ 50 ppm). In both cases, Freudlich and Langmuir models do not fit well the data, indicating the more complicated mechanism taking place during adsorption rather than monolayer or multilayer adsorption. As shown at Fig. 6(a), at the range of $C_0 <$ 50 ppm, the Sips isotherm fits better with the empirical data. The Sips isotherm (Equation (4)) [67,68] is deduced from the limiting behavior of the Langmuir and Freundlich models and it is appropriate for estimating adsorption on heterogeneous surfaces. The model is reliable for localized sorption without adsorbate–adsorbate interplays [69].

$$q_e = q_{max}\frac{(K_sC_e)^n}{1+(K_sC_e)^n} \quad (4)$$

where K_s (l/mg) and q_{max} (mg/g) represent the Sips equilibrium constant and maximum adsorption capacity, C_e is the concentration at the equilibrium, while n is the dimensionless heterogeneity factor that explains the system's heterogeneity when n is between 0 and 1. When n = 1, the Sips model approaches the Langmuir theory which connotes a homogeneous adsorption behavior on a monolayer [70]. Therefore, as presented in Fig. 6(a), considering the heterogeneity factor value for Sips model, which is close to 1, Langmuir theory better defines the adsorption mechanism up to initial PFBS concentrations of c.a. 50 ppm. Consequently, it can be comprehended that within the concentration range studied, maximum adsorption occurs when a saturated monolayer of PFBS molecules is formed on the xerogel surface, the sorption energy remains unchanged, and no relocation or interaction between the PFBS molecules occurs on the surface of the sorbent.

As the PFBS C_0 increases, adsorption behavior changes and the Sips isotherm is no longer able to correlate the data. After comprehensive analysis, Temkin isotherm showed the best conformity with the experimental data (Fig. 6(b)). The Temkin isotherm model can be expressed as [71]:

$$q_e = \frac{RT}{b_T}\ln(A_TC_e) \quad (5)$$

where R, T, b_T, and A_T represent universal gas constant (8.314 J mol^{-1} K^{-1}), temperature (K), Temkin isotherm constant, which considers adsorbent-adsorbate chemical interactions, and Temkin isotherm equilibrium binding constant (l/mg), respectively. Temkin isotherm

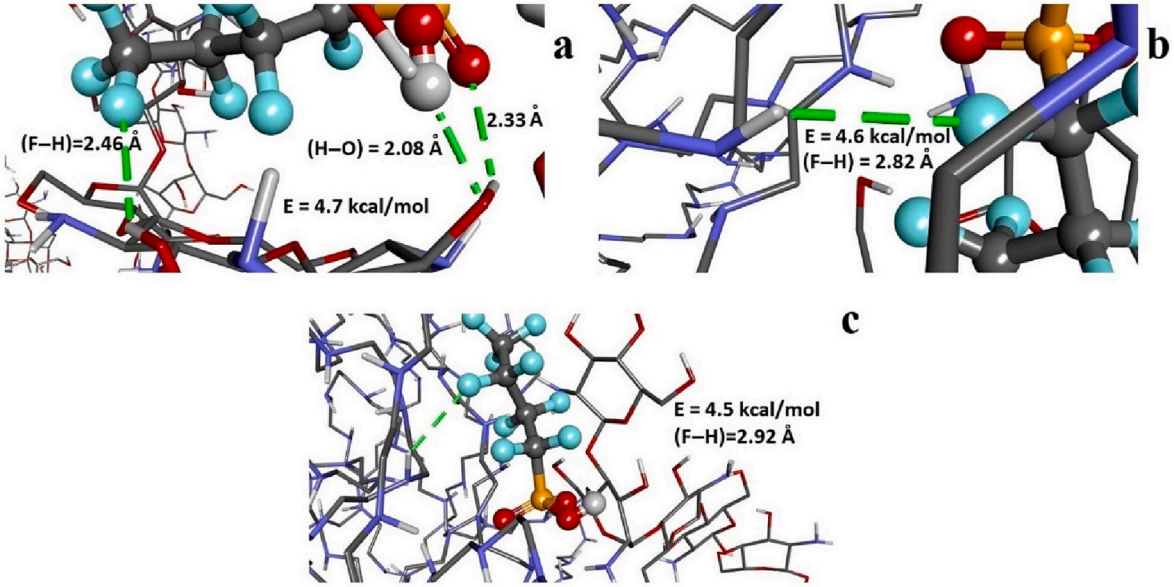

Fig. 7. The best configurations of PFBS molecules in adsorbed phase among the polymer chains: CS (a), PEI (b), and both CS and PEI (c); nitrogen atoms are in blue, fluorine atoms in light blue, sulfur atoms in yellow, oxygen atoms in red, hydrogen atoms in light grey, and carbon atoms in grey; the distance between atoms illustrated in the figure indicates the length of H-bond which can represent the strength of hydrogen bonds. (For interpretation of the references to colour in this figure legend, the reader is referred to the web version of this article.)

indicates that the sorption sites accommodate more than a layer of adsorbate and not all adsorbed molecules are in direct contact with the top layer of the adsorbent [72]. From the fitting parameters listed in Table S3 the b_T value is c.a. 8 J/mol specifying that, in the studied concentration range, physisorption of the PFBS molecules occurs on the CS/PEI xerogel [73]. In fact, Temkin isotherm suggests that electrostatic interactions between adsorbent and adsorbate occur [73,74], consistent with the presence of probable charge-assisted hydrogen bond interactions between PFBS and PEI/CS [75]. Therefore, it can be concluded that in lower PFBS concentrations, formation of a monolayer adsorbate on the surface of the adsorbent is a dominant factor while in higher concentrations a multilayer adsorption process [76] controls the PFBS adsorption.

To discover the composite attributes and prove the affinity of the adsorbent towards the target molecule, adsorbent-adsorbate interactions were also evaluated by molecular docking studies. The most probable configurations of adsorbent-adsorbate (receptor-ligand) obtained from the docking process are visualized in Fig. 7. In particular, are depicted possible configurations of the PFBS molecules in the presence of the polymer chains, as also the presence of possible interactions between PFBS and active sites on the adsorbent's surface. In particular, Fig. 7 shows the most possible configuration of the PFBS molecule with the individual CS and PEI chains and of the composite xerogel with the most stable interactions. According to the docking results, the PFBS molecule can interact with the amine and hydroxyl functional groups of both types of polymer chains of the composite xerogel. In particular, as can be observed, the –NH groups on both PEI and CS chains and the –OH groups of the CS can be considered as active sites of the adsorbent and are the most potent sites to create hydrogen bonds. In fact, as shown, the F and O atoms of the PFBS molecule give rise to binding pose with the H atoms of the prepared xerogel or the H atom of PFBS with the hydroxyl groups of the adsorbent due to their high electronegativity. The intensity of intermolecular interaction has been computed to be between 4.5 and 4.7 kcal/mol, which demonstrates strong affinity of the polymeric composite toward PFBS molecules. This high affinity can be also proved from the H- bond length which is$<$3 Å in all cases. Such values indicate the presence of "strong, mostly covalent" H–bonds (when the bond length is in the range of 2.2–2.5 Å) and "moderate, mostly electrostatic" H–bonds (when the bond length is in the range of 2.5–3.2 Å) based on the Jeffrey's classification [77]. In fact, as also proved by the FTIR analysis, possible hydrogen bindings between the amine groups of the xerogel with the fluorine atom of PFBS cause a shifting in the position of C–N stretching peak after adsorption. It is worth mentioning that repulsion of acceptor–acceptor (between two oxygen atoms) is also probable which is not beneficial. Therefore, according to the intermolecular energies estimated by molecular docking, the high affinity of the prepared xerogel to the PFBS molecules has been confirmed, in accordance with the FTIR and XPS analysis described before.

4. Conclusion

Highly porous CS/PEI composite xerogels have been successfully synthesized via a cryogelation process in the presence of BDDE as crosslinking agent, and their ability to uptake PFBS molecules was assessed within a broad range of concentrations. After the detailed characterization, it is proved that the xerogel is able to adsorb PFBS molecules with a maximum adsorption capacity of c.a. 305 $\pm$ 45 mg/g. The interaction of the PFBS molecules with the xerogel's surface is proved to occur through electrostatic interactions along with the formation of hydrogen bonds as also confirmed by the molecular docking simulations. In case of adsorption mechanisms, two different behaviors were observed. In particular, at low to moderate PFBS concentrations, a monolayer of the adsorbate on the surface of the xerogel controls the process while at higher concentrations multilayer sorption plays a key role in the PFBS adsorption. Considering their great adsorption capacity, CS/PEI composite xerogels may be potential adsorbents for the removal of short-chain PFBS from aqueous media.

Declaration of Competing Interest

The authors declare that they have no known competing financial interests or personal relationships that could have appeared to influence the work reported in this paper.

Data availability

No data was used for the research described in the article.

Acknowledgements

The authors thank Lara Marini for the TGA analysis and Lea Pasquale for gas sorption analysis.

Appendix A. Supplementary data

Supplementary data to this article can be found online at https://doi.org/10.1016/j.cej.2023.143236.

References

[1] P.-J. Huang, M. Hwangbo, Z. Chen, Y. Liu, J. Kameoka, K.-H. Chu, Reusable functionalized hydrogel sorbents for removing long-and short-chain perfluoroalkyl acids (PFAAs) and GenX from aqueous solution, ACS omega 3 (12) (2018) 17447–17455.
[2] A. Podder, A.A. Sadmani, D. Reinhart, N.-B. Chang, R. Goel, Per and poly-fluoroalkyl substances (PFAS) as a contaminant of emerging concern in surface water: a transboundary review of their occurrences and toxicity effects, Journal of hazardous materials 419 (2021), 126361.
[3] T. Wu, Z. Wu, D. Ma, W. Xiang, J. Zhang, H. Liu, Y. Deng, S. Tan, X. Cai, Fabrication of few-layered porous graphite for removing fluorosurfactant from aqueous solution, Langmuir 34 (50) (2018) 15181–15188.
[4] C.M. Butt, D.C.G. Muir, S.A. Mabury, Biotransformation pathways of fluorotelomer-based polyfluoroalkyl substances: A review, Environmental toxicology and chemistry 33 (2) (2014) 243–267.
[5] K. Prevedouros, I.T. Cousins, R.C. Buck, S.H. Korzeniowski, Sources, fate and transport of perfluorocarboxylates, Environmental science & technology 40 (1) (2006) 32–44.
[6] S. Kurwadkar, J. Dane, S.R. Kanel, M.N. Nadagouda, R.W. Cawdrey, B. Ambade, G. C. Struckhoff, R. Wilkin, Per-and polyfluoroalkyl substances in water and wastewater: A critical review of their global occurrence and distribution, Science of The Total Environment 809 (2022), 151003.
[7] M.-J. Lopez-Espinosa, D. Mondal, B. Armstrong, M.S. Bloom, T. Fletcher, Thyroid function and perfluoroalkyl acids in children living near a chemical plant, Environmental health perspectives 120 (7) (2012) 1036–1041.
[8] Y. Shi, X. Song, Q. Jin, W. Li, S. He, Y. Cai, Tissue distribution and bioaccumulation of a novel polyfluoroalkyl benzenesulfonate in crucian carp, Environment international 135 (2020), 105418.
[9] A.B. Lindstrom, M.J. Strynar, E.L. Libelo, J.A. Field, Guest comment: Perfluoroalkyl acid focus issue, ACS Publications 45 (19) (2011) 7951–7953.
[10] G.W. Olsen, J.M. Burris, D.J. Ehresman, J.W. Froehlich, A.M. Seacat, J. L. Butenhoff, L.R. Zobel, Half-life of serum elimination of perfluorooctanesulfonate, perfluorohexanesulfonate, and perfluorooctanoate in retired fluorochemical production workers, Environmental health perspectives 115 (9) (2007) 1298–1305.
[11] J. Bao, W.-J. Yu, Y. Liu, X. Wang, Z.-Q. Liu, Y.-F. Duan, Removal of perfluoroalkanesulfonic acids (PFSAs) from synthetic and natural groundwater by electrocoagulation, Chemosphere 248 (2020), 125951.
[12] S.P. Lenka, M. Kah, L.P. Padhye, A review of the occurrence, transformation, and removal of poly-and perfluoroalkyl substances (PFAS) in wastewater treatment plants, Water research 199 (2021), 117187.
[13] Q. Luo, S. Liang, Q. Huang, Laccase induced degradation of perfluorooctanoic acid in a soil slurry, Journal of hazardous materials 359 (2018) 241–247.
[14] M. Pierpaoli, M. Szopińska, B.K. Wilk, M. Sobaszek, A. Łuczkiewicz, R. Bogdanowicz, S. Fudala-Książek, Electrochemical oxidation of PFOA and PFOS in landfill leachates at low and highly boron-doped diamond electrodes, Journal of Hazardous Materials 403 (2021), 123606.
[15] J. Wang, L. Wang, C. Xu, R. Zhi, R. Miao, T. Liang, X. Yue, Y. Lv, T. Liu, Perfluorooctane sulfonate and perfluorobutane sulfonate removal from water by nanofiltration membrane: The roles of solute concentration, ionic strength, and macromolecular organic foulants, Chemical Engineering Journal 332 (2018) 787–797.
[16] K.E. Carter, J. Farrell, Removal of perfluorooctane and perfluorobutane sulfonate from water via carbon adsorption and ion exchange, Separation Science and Technology 45 (6) (2010) 762–767.
[17] Z. Du, S. Deng, Y. Bei, Q. Huang, B. Wang, J. Huang, G. Yu, Adsorption behavior and mechanism of perfluorinated compounds on various adsorbents—A review, Journal of hazardous materials 274 (2014) 443–454.
[18] E. Gagliano, M. Sgroi, P.P. Falciglia, F.G. Vagliasindi, P. Roccaro, Removal of poly-and perfluoroalkyl substances (PFAS) from water by adsorption: Role of PFAS chain length, effect of organic matter and challenges in adsorbent regeneration, Water research 171 (2020), 115381.
[19] N. Merino, Y. Qu, R.A. Deeb, E.L. Hawley, M.R. Hoffmann, S. Mahendra, Degradation and removal methods for perfluoroalkyl and polyfluoroalkyl substances in water, Environmental Engineering Science 33 (9) (2016) 615–649.
[20] C.A. Clark, K.N. Heck, C.D. Powell, M.S. Wong, Highly defective UiO-66 materials for the adsorptive removal of perfluorooctanesulfonate, ACS Sustainable Chemistry & Engineering 7 (7) (2019) 6619–6628.
[21] R. Li, S. Alomari, R. Stanton, M.C. Wasson, T. Islamoglu, O.K. Farha, T.M. Holsen, S.M. Thagard, D.J. Trivedi, M. Wriedt, Efficient removal of per-and polyfluoroalkyl substances from water with zirconium-based metal–organic frameworks, Chemistry of Materials 33 (9) (2021) 3276–3285.
[22] S. Tang, X. Qin, Y. Lv, K. Hu, S. Zhao, Adsorption of three perfluoroalkyl sulfonate compounds from environmental water and human serum samples using cationic porous covalent organic framework as adsorbents and detection combination with MALDI-TOF MS, Applied Surface Science 601 (2022), 154224.
[23] W. Wang, H. Shao, S. Zhou, D. Zhu, X. Jiang, G. Yu, S. Deng, Rapid removal of perfluoroalkanesulfonates from water by β-cyclodextrin covalent organic frameworks, ACS Applied Materials & Interfaces 13 (41) (2021) 48700–48708.
[24] J. Cheng, C.D. Vecitis, H. Park, B.T. Mader, M.R. Hoffmann, Sonochemical degradation of perfluorooctane sulfonate (PFOS) and perfluorooctanoate (PFOA) in landfill groundwater: environmental matrix effects, Environmental science & technology 42 (2008) 8057–8063.
[25] L. Jin, P. Zhang, Photochemical decomposition of perfluorooctane sulfonate (PFOS) in an anoxic alkaline solution by 185 nm vacuum ultraviolet, Chemical Engineering Journal 280 (2015) 241–247.
[26] M. Ateia, M. Arifuzzaman, S. Pellizzeri, M.F. Attia, N. Tharayil, J.N. Anker, T. Karanfil, Cationic polymer for selective removal of GenX and short-chain PFAS from surface waters and wastewaters at ng/L levels, Water research 163 (2019), 114874.
[27] A.H. Karoyo, L.D. Wilson, Tunable macromolecular-based materials for the adsorption of perfluorooctanoic and octanoic acid anions, Journal of colloid and interface science 402 (2013) 196–203.
[28] S. Kawano, T. Kida, S. Takemine, C. Matsumura, T. Nakano, M. Kuramitsu, K. Adachi, M. Akashi, Efficient removal and recovery of perfluorinated compounds from water by surface-tethered β-cyclodextrins on polystyrene particles, Chemistry Letters 42 (4) (2013) 392–394.
[29] C. Xu, H. Chen, F. Jiang, Adsorption of perflourooctane sulfonate (PFOS) and perfluorooctanoate (PFOA) on polyaniline nanotubes, Colloids and Surfaces A: Physicochemical and Engineering Aspects 479 (2015) 60–67.
[30] R.R. Navarro, K. Sumi, N. Fujii, M. Matsumura, Mercury removal from wastewater using porous cellulose carrier modified with polyethyleneimine, Water Research 30 (10) (1996) 2488–2494.
[31] S.W. Won, J. Park, J. Mao, Y.-S. Yun, Utilization of PEI-modified Corynebacterium glutamicum biomass for the recovery of Pd (II) in hydrochloric solution, Bioresource Technology 102 (4) (2011) 3888–3893.
[32] S. Wong, H.H. Tumari, N. Ngadi, N.B. Mohamed, O. Hassan, R. Mat, N.A.S. Amin, Adsorption of anionic dyes on spent tea leaves modified with polyethyleneimine (PEI-STL), Journal of cleaner production 206 (2019) 394–406.
[33] C. Zhang, X. Wang, J. Lin, B. Ding, J. Yu, N. Pan, Nanoporous polystyrene fibers functionalized by polyethyleneimine for enhanced formaldehyde sensing, Sensors and Actuators B: Chemical 152 (2011) 316–323.
[34] M. Ateia, M.F. Attia, A. Maroli, N. Tharayil, F. Alexis, D.C. Whitehead, T. Karanfil, Rapid removal of poly-and perfluorinated alkyl substances by poly (ethylenimine)-functionalized cellulose microcrystals at environmentally relevant conditions, Environmental Science & Technology Letters 5 (12) (2018) 764–769.
[35] B. Hastuti, A. Masykur, S. Hadi, Modification of chitosan by swelling and crosslinking using epichlorohydrin as heavy metal Cr (VI) adsorbent in batik industry wastes, in: IOP Conference Series: Materials Science and Engineering, IOP Publishing, 2016, p. 012020.
[36] H. Yan, Y. Feng, W. Hu, C. Cheng, R. Liu, C. Wang, J. Li, Q. Lin, Preparation and evaluation of alginate-chitosan-bentonite based beads for the delivery of pesticides in controlled-release formulation, Asian Journal of Chemistry 25 (17) (2013) 9936–9940.
[37] S. Subramani, N. Thinakaran, Isotherm, kinetic and thermodynamic studies on the adsorption behaviour of textile dyes onto chitosan, Process Safety and Environmental Protection 106 (2017) 1–10.
[38] M. Mahmoud Nasef, E.A. El-Hefian, S. Saalah, A.H. Yahaya, Preparation and properties of non-crosslinked and ionically crosslinked chitosan/agar blended hydrogel films, E-Journal of, Chemistry 8 (2011) S409–S419.
[39] Q. Zhang, S. Deng, G. Yu, J. Huang, Removal of perfluorooctane sulfonate from aqueous solution by crosslinked chitosan beads: sorption kinetics and uptake mechanism, Bioresource technology 102 (2011) 2265–2271.
[40] F. Banisheykholeslami, M. Hosseini, G.N. Darzi, Design of PAMAM grafted chitosan dendrimers biosorbent for removal of anionic dyes: adsorption isotherms, kinetics and thermodynamics studies, International Journal of Biological Macromolecules 177 (2021) 306–316.
[41] M. Gouamid, M. Ouahrani, M. Bensaci, Adsorption equilibrium, kinetics and thermodynamics of methylene blue from aqueous solutions using date palm leaves, Energy procedia 36 (2013) 898–907.
[42] H. Sun, COMPASS: an ab initio force-field optimized for condensed-phase applications overview with details on alkane and benzene compounds, The Journal of Physical Chemistry B 102 (1998) 7338–7364.
[43] O. Trott, A.J. Olson, AutoDock Vina: improving the speed and accuracy of docking with a new scoring function, efficient optimization, and multithreading, Journal of computational chemistry 31 (2010) 455–461.
[44] D.S. Saini, S. Tripathy, A. Kumar, S.K. Sharma, A. Ghosh, D. Bhattacharya, Impedance and modulus spectroscopic analysis of single phase BaZrO 3 ceramics for SOFC application, Ionics 24 (4) (2018) 1161–1171.
[45] G. Horvat, M. Pantić, Ž. Knez, Z. Novak, A Brief Evaluation of Pore Structure Determination for Bioaerogels, Gels 8 (2022) 438.
[46] Z. Chen, Z.-B. Zhang, J. Zeng, Z.-J. Zhang, S. Ma, C.-M. Tang, J.-Q. Xu, Preparation of polyethyleneimine-modified chitosan/Ce-UIO-66 composite hydrogel for the adsorption of methyl orange, Carbohydrate Polymers 299 (2023), 120079.
[47] J. Zhang, Y. Li, Y. Dai, T. Lin, H. Shao, Y. Liu, X. Liu, Three-dimensional porous hydrogel based on hyperbranched polyethyleneimine functionalized apple pomace

derived cellulose for efficient removal of methyl orange, Chemical Engineering Journal 456 (2023), 140995.
[48] X. Zeng, G. Zhang, J. Wen, X. Li, J. Zhu, Z. Wu, Simultaneous removal of aqueous same ionic type heavy metals and dyes by a magnetic chitosan/polyethyleneimine embedded hydrophobic sodium alginate composite: Performance, interaction and mechanism, Chemosphere 318 (2023), 137869.
[49] S.-L. Loo, W.B. Krantz, T.-T. Lim, A.G. Fane, X. Hu, Design and synthesis of ice-templated PSA cryogels for water purification: towards tailored morphology and properties, Soft Matter 9 (2013) 224–234.
[50] X. Xu, J.M. Andresen, C. Song, B.G. Miller, A.W. Scaroni, Preparation of novel CO2" molecular basket" of polymer modified MCM-41, ACS Division of Fuel Chemistry, Preprints 47 (2002) 67–68.
[51] B. Lim, C. Poh, C.H. Voon, H. Salmah, Rheological and thermal study of chitosan filled thermoplastic elastomer composites, Trans Tech Publ, Applied Mechanics and Materials, 2015, pp. 34–38.
[52] E.S. Dragan, D. Humelnicu, M.V. Dinu, Development of chitosan-poly (ethyleneimine) based double network cryogels and their application as superadsorbents for phosphate, Carbohydrate polymers 210 (2019) 17–25.
[53] M.F. Queiroz, K.R. Teodosio Melo, D.A. Sabry, G.L. Sassaki, H.A.O. Rocha, Does the use of chitosan contribute to oxalate kidney stone formation? Marine drugs 13 (2014) 141–158.
[54] Z.-T. Li, J. Guo, J.-S. Zhang, Y.-P. Zhao, L.u. Lv, C. Ding, X.-Z. Zhang, Chitosan-graft-polyethylenimine with improved properties as a potential gene vector, Carbohydrate Polymers 80 (1) (2010) 254–259.
[55] K. Grenda, A. Idström, L. Evenäs, M. Persson, K. Holmberg, R. Bordes, An analytical approach to elucidate the architecture of polyethyleneimines, Journal of Applied Polymer Science 139 (2022) 51657.
[56] M.R.S. Kebria, M. Jahanshahi, A. Rahimpour, SiO2 modified polyethyleneimine-based nanofiltration membranes for dye removal from aqueous and organic solutions, Desalination 367 (2015) 255–264.
[57] G. Lawrie, I. Keen, B. Drew, A. Chandler-Temple, L. Rintoul, P. Fredericks, L. Grøndahl, Interactions between alginate and chitosan biopolymers characterized using FTIR and XPS, Biomacromolecules 8 (8) (2007) 2533–2541.
[58] M.R.S. Kebria, Nanofiltration membranes synthesized from polyethyleneimine for removal of MgSO4 from aqueous solution (RESEARCH NOTE), International Journal of Engineering 27 (2014) 1173–1178.
[59] S. Mincke, T.G. Asere, I. Verheye, K. Folens, F. Vanden Bussche, L. Lapeire, K. Verbeken, P. Van Der Voort, D.A. Tessema, F. Fufa, G. Du Laing, C.V. Stevens, Functionalized chitosan adsorbents allow recovery of palladium and platinum from acidic aqueous solutions, Green Chemistry 21 (9) (2019) 2295–2306.
[60] P. Sriprapha, N. Kapao, A. Chaijaruwanich, Characterization of Physical Properties and Tensile Strength of Chitosan/Fibroin Composite via Freeze Drying Method, IOP Conf. Ser.: Mater. Sci. Eng. 639 (1) (2019) 012007.
[61] L. Vanzetti, L. Pasquardini, C. Potrich, V. Vaghi, E. Battista, F. Causa, C. Pederzolli, XPS analysis of genomic DNA adsorbed on PEI-modified surfaces, Surface and Interface Analysis 48 (2016) 611–615.
[62] D.-M. Guo, Q.-D. An, Z.-Y. Xiao, S.-R. Zhai, Z. Shi, Polyethylenimine-functionalized cellulose aerogel beads for efficient dynamic removal of chromium (VI) from aqueous solution, RSC advances 7 (2017) 54039–54052.
[63] X. Tian, W. Wang, Y. Wang, S. Komarneni, C. Yang, Polyethylenimine functionalized halloysite nanotubes for efficient removal and fixation of Cr (VI), Microporous and Mesoporous Materials 207 (2015) 46–52.
[64] X. Gao, J. Chorover, Adsorption of perfluorooctanoic acid and perfluorooctanesulfonic acid to iron oxide surfaces as studied by flow-through ATR-FTIR spectroscopy, Environmental Chemistry 9 (2012) 148–157.
[65] B.D. Turner, S.W. Sloan, G.R. Currell, Novel remediation of per-and polyfluoroalkyl substances (PFASs) from contaminated groundwater using Cannabis Sativa L. (hemp) protein powder, Chemosphere 229 (2019) 22–31.
[66] L. Campagnolo, D. Morselli, D. Magrì, A. Scarpellini, C. Demirci, M. Colombo, A. Athanassiou, D. Fragouli, Silk fibroin/orange peel foam: an efficient biocomposite for water remediation, Advanced Sustainable Systems 3 (1) (2019) 1800097.
[67] F. Banisheykholeslami, A.A. Ghoreyshi, M. Mohammadi, K. Pirzadeh, Synthesis of a carbon molecular sieve from broom corn stalk via carbon deposition of methane for the selective separation of a CO2/CH4 mixture, CLEAN–Soil, Air, Water 43 (2015) 1084–1092.
[68] F. Banisheykholeslami, M. Hosseini, G.N. Darzi, M.R.S. Kebria, Design of novel hyper-branched dendritic boehmite/gallic acid alumoxane for methylene blue removal: Adsorption mechanism and reusability, Korean Journal of Chemical Engineering (2023) 1–13.
[69] K.Y. Foo, B.H. Hameed, Insights into the modeling of adsorption isotherm systems, Chemical engineering journal 156 (1) (2010) 2–10.
[70] N.T.R.N. Kumara, N. Hamdan, M.I. Petra, K.U. Tennakoon, P. Ekanayake, Equilibrium isotherm studies of adsorption of pigments extracted from Kuduk-kuduk (Melastoma malabathricum L.) pulp onto TiO2 nanoparticles, Journal of Chemistry 2014 (2014) 1–6.
[71] A. Dada, A. Olalekan, A. Olatunya, O. Dada, Langmuir, Freundlich, Temkin and Dubinin-Radushkevich isotherms studies of equilibrium sorption of Zn2+ unto phosphoric acid modified rice husk, IOSR Journal of applied chemistry 3 (2012) 38–45.
[72] A. Inyinbor, F. Adekola, G.A. Olatunji, Kinetics, isotherms and thermodynamic modeling of liquid phase adsorption of Rhodamine B dye onto Raphia hookerie fruit epicarp, Water Resources and Industry 15 (2016) 14–27.
[73] M.N. Ettish, G.S. El-Sayyad, M.A. Elsayed, O. Abuzalat, Preparation and characterization of new adsorbent from Cinnamon waste by physical activation for removal of Chlorpyrifos, Environmental challenges 5 (2021), 100208.
[74] P.K. Sharma, S. Ayub, C.N. Tripathi, Isotherms describing physical adsorption of Cr (VI) from aqueous solution using various agricultural wastes as adsorbents, Cogent Engineering 3 (2016) 1186857.
[75] P. Trujillo, T. González, J.L. Brito, A. Briceño, Surface recognition directed selective removal of dyes from aqueous solution on hydrophilic functionalized petroleum coke sorbents. A supramolecular perspective, Industrial & Engineering Chemistry Research 58 (32) (2019) 14761–14774.
[76] S. Kalam, S.A. Abu-Khamsin, M.S. Kamal, S. Patil, Surfactant adsorption isotherms: A review, ACS omega 6 (48) (2021) 32342–32348.
[77] G.A. Jeffrey, G.A. Jeffrey, An introduction to hydrogen bonding, Oxford University Press, New York, 1997.